Electronic Supporting Information

Simple Construction of Deep-Red Hexaazatrinaphthylene-Based Thermally Activated Delayed Fluorescence Emitters for Efficient Solution-Processed OLEDs with Peak at 692 nm

Xue Zhou,[a,b] Yepeng Xiang,[b] Shaolong Gong,*[b] Zhanxiang Chen,[b] Fan Ni, [a] Guohua Xie[b] and Chuluo Yang*[a,b]

[a] *Shenzhen Key Laboratory of Polymer Science and Technology, College of Materials Science and Engineering, Shenzhen University, Shenzhen, 518060, People's Republic of China, E-mail: clyang@whu.edu.cn.*

[b] *Hubei Key Lab on Organic and Polymeric Optoelectronic Materials, Department of Chemistry, Wuhan University, Wuhan, 430072, People's Republic of China. E-mail: slgong@whu.edu.cn.*

Materials and instrument

All chemical reagents were purchased from commercial chemical companies and used without further purification unless it was necessary. The reactions and manipulations susceptive to moisture and oxygen were carried out under the protection of argon. The 400 MHz ^{1}H and 100 MHz ^{13}C nuclear magnetic resonance (NMR) spectra were recorded on a Bruker AV-500 (400 MHz) in deuterated chloroform with tetramethyl-silane (TMS) as an internal reference. MALDI-TOF mass spectrometric measurements were performed on 5800MALDITOF (AB SCIEX, USA) mass spectrometer. Thermogravimetric analysis (TGA) was recorded on a NEZSCH STA 449C instrument under nitrogen atmosphere at a heating rate of 10 ^{o}C/min from 25 ^{o}C to 800 ^{o}C. The temperature of degradation (T_d) was correlated to a 5% weight loss. Cyclic voltammetry (CV) data were measured on a CHI630E electrochemical workstation equipped with a glassy carbon working electrode, a saturated calomel electrode as the reference

electrode, and a platinum wire counter electrode. The measurements were carried out with anhydrous acetonitrile tetrabutylammoniumhexafluorophosphate (0.1 M) as the supporting electrolyte at a scan rate of 100 mV s^{-1}. Potentials were referenced to the ferrocene/ferrocenium couple by using ferrocene as the standard. The fermi level of ferrocene was set at -4.80 eV with respect to zero vacuum level. The measurement of atomic force microscope (AFM) was carried out with an Oxford instruments spm-9700. UV-vis absorption spectra were obtained with a Shimadzu UV-3600 UV-vis-NIR spectrometer. Photoluminescence (PL) spectra were recorded on a Hitachi F-4600 fluorescence spectrophotometer. The PL lifetimes were measured by a single photon counting spectrometer from Edinburgh Instruments (FLS920) with a Picosecond Pulsed UV-LASTER (LASTER377) as the excitation source. The samples were placed in a vacuum cryostat chamber with the temperature control. The solid state absolute PLQYs were measured on a Quantaurus-QY measurement system (C9920-02, Hamamatsu Photonics) equipped with a calibrated integrating sphere in neat films and all the samples were excited at 310 nm. The ground state molecular structures were optimized at the B3LYP/def2-SVP level of theory. Energy gaps between first singlet state (S_1) and triplet state (T_1) were calculated using the TD-DFT based on the PBE0/def2-SVP level of theory on the optimized geometry.

Device fabrication and characterization

The prepatterned indium tin oxide (ITO) substrates were cleaned by ultrasonic acetone bath, followed by ethanol bath. Afterward, the substrates were dried with N_2 and then loaded into a UV-Ozone chamber. After UV-Ozone treatment, the PEDOT:PSS layer was spin-coated on the ITO substrate at 4000 rpm as the hole-injecting layer. The substrate was transferred into a N_2 filled glove box and then annealed at 120 °C for 10 min to remove the residual solvent. The emissive layer was prepared by spin-coating directly on the hole-injecting layer at 1000 rpm, and then annealed at 50 °C for 10 min. The electron-transporting material, the electron injecting materials and the cathode material were consecutively evaporated in a vacuum chamber under 10^{-5} mbar. Before

being taken out of the glovebox, the devices were encapsulated with UV-curable epoxy. The voltage-current-luminance characteristics and the electroluminescence (EL) spectra were simultaneously measured with PR735 SpectraScan Photometer and Keithley 2400 sourcemeter unit under ambient atmosphere at room temperature. The EQE was calculated from the current density, luminance and EL spectrum, assuming a Lambertian distribution.

Synthesis of 2,3,8,9,14,15-Hexa-[3,6-Bis(4-*tert*-butyl)carbazol]-5,6,11,12,17,18-hexaazatrinaphthylene (HATNA-tCz): 3,6-Di-*tert*-butylcarbazole (2.52 g, 9 mmol) and potassium *tert*-butoxide (1.01g, 9 mmol) was added into 20 mL dry *N, N*-dimethyl formamide and reacted at 50 ^{o}C under argon for 2 hours. And then HATNA-6F (0.50 g, 1 mmol) was added into the reaction mixture and refluxed under argon for 72 h. After cooling to room temperature, the mixture was poured into water, extracted with dichloromethane three times (50 mL×3), dried and then concentrated in vacuum. The crude product was purified by column chromatography on silica gel using petroleum ether/DCM (1:1 v/v) as the eluent to give a crimson solid (0.79 g, yield: 39%). ^{1}H NMR (400 MHz, $CDCl_3$+TMS, 298 K) δ [ppm]: 9.21 (s, 6H), 7.62 (s, 12H), 7.03 (d, J = 8.6 Hz, 12H), 6.91 (d, J = 8.4 Hz, 12H), 1.35 (s, 108H). ^{13}C NMR (101 MHz, $CDCl_3$, 298 K) δ [ppm]: 144.13, 143.62, 143.04, 139.11, 137.76, 130.71, 124.03, 122.98, 115.45, 109.02, 34.55, 31.88. MS (MALDI-TOF, m/z): calcd. for $C_{144}H_{150}N_{12}$ [M^+]: 2048.21; Found: 2048.26.

Synthesis of 2,3,8,9,14,15-Hexa-[3,6-Bis(4-*tert*-butylphenyl)carbazol]-5,6,11,12,17,18-hexaazatrinaphthylene (HATNA-tPCz): The synthetic procedure of HATNA-tPCz was similar to that of HATNA-tCz with replacing 3,6-Di-*tert*-butylcarbazole with same equal 3,6-Bis(4-*tert*-butylphenyl)carbazole to afford a red and black solid (1.05 g, yield: 48%). ^{1}H NMR (400 MHz, $CDCl_3$+TMS, 298 K) δ [ppm]: 9.26 (s, 6H), 7.90 (s, 12H), 7.44-7.25 (m, 72H), 1.31 (s, 108H). ^{13}C NMR (100 MHz, $CDCl_3$, 298 K) δ [ppm]: 149.50, 144.34, 142.90, 139.22, 138.38, 134.02, 131.22,

128.63, 126.72, 125.58, 124.83, 124.55, 118.15, 110.00, 34.39, 31.34. MS (MALDI-TOF, m/z): calcd. for $C_{216}H_{198}N_{12}$ [M^+]: 2961.59; Found: 2961.62.

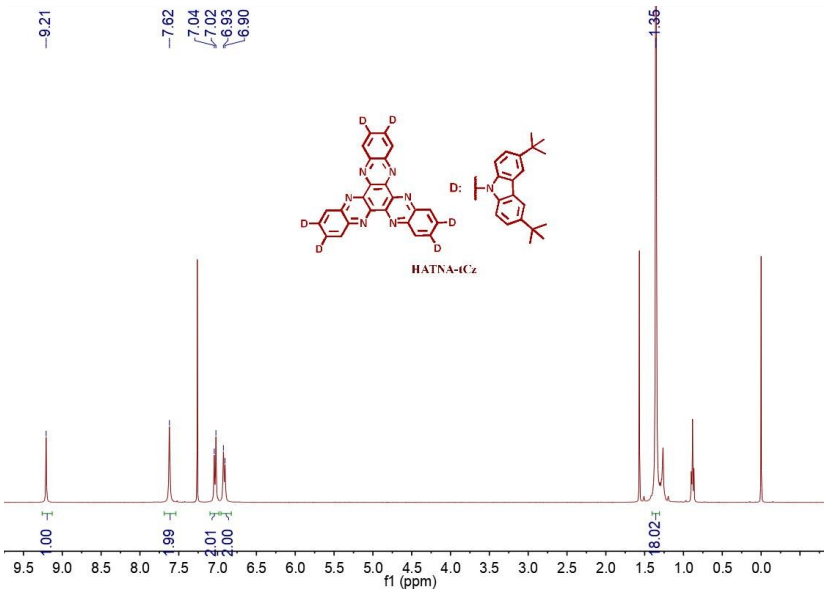

Fig. S1 ^{1}H NMR spectrum of HATNA-tCz (400 MHz, $CDCl_3$ + TMS, 298 K).

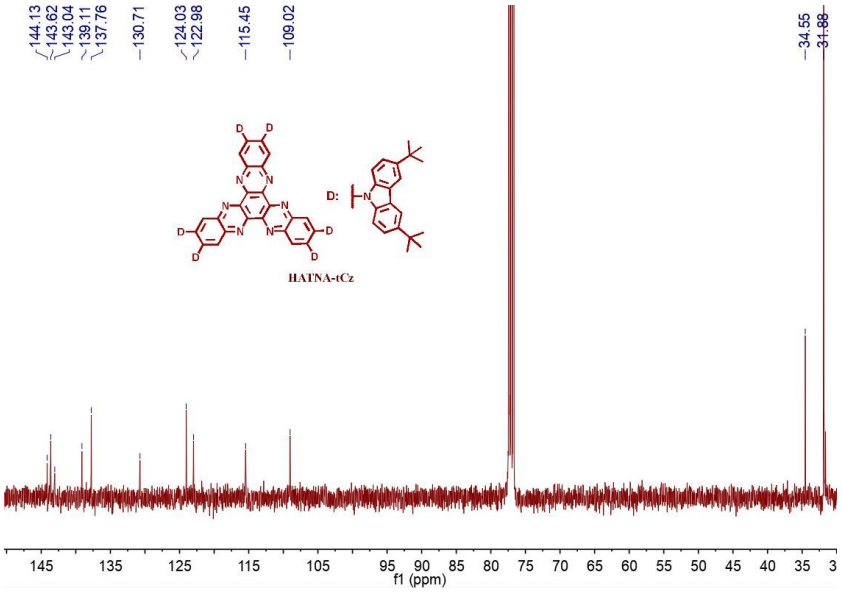

Fig. S2 ^{13}C NMR spectrum of HATNA-tCz (100 MHz, $CDCl_3$, 298 K).

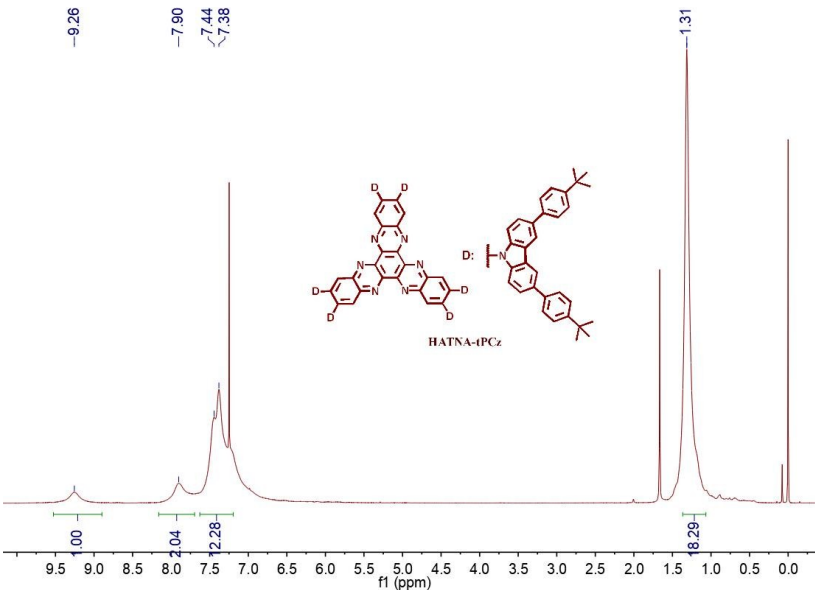

Fig. S3 ^{1}H NMR spectrum of HATNA-tPCz (400 MHz, $CDCl_3$ + TMS, 298 K).

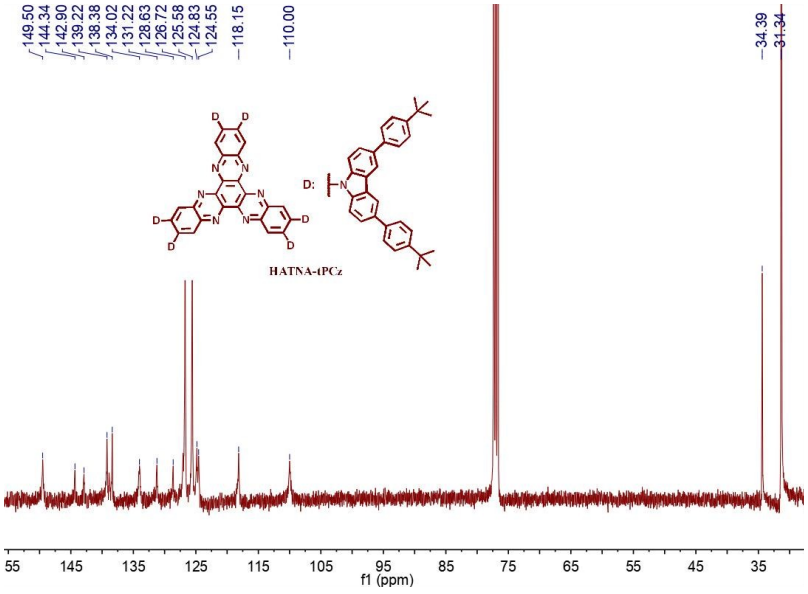

Fig. S4 ^{13}C NMR spectrum of HATNA-tPCz (100 MHz, $CDCl_3$, 298 K).

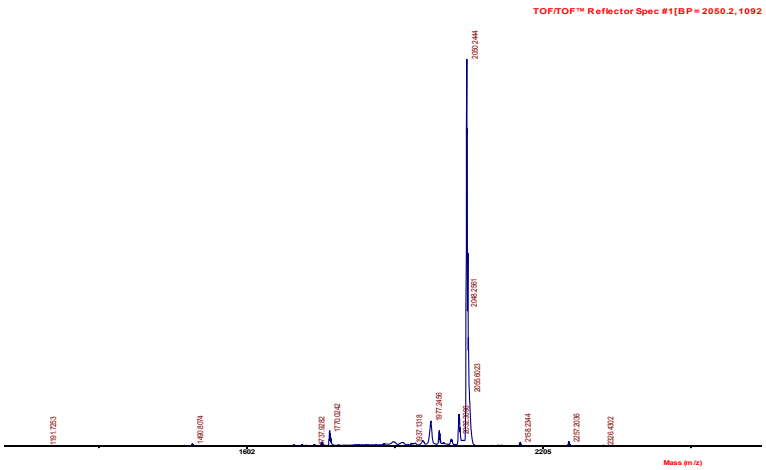

Fig. S5 MALDI-TOF spectrum of HATNA-tCz.

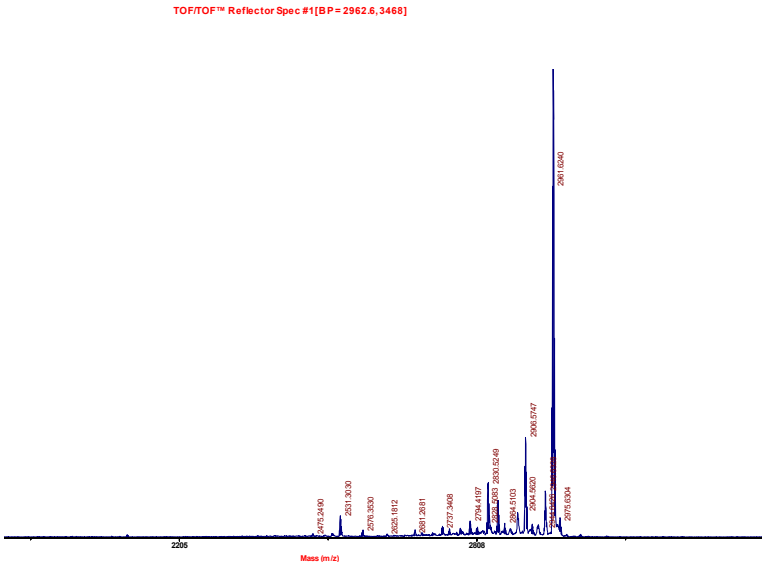

Fig. S6 MALDI-TOF spectrum of HATNA-tPCz.

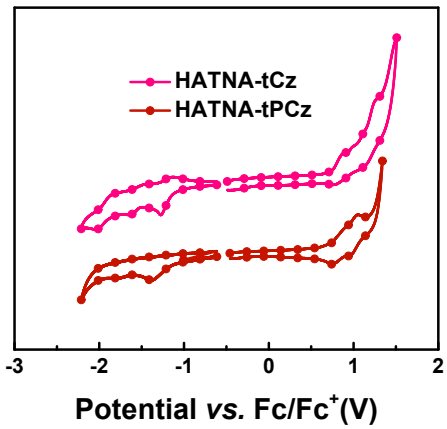

Fig. S7 Oxidation and reduction behaviors of HATNA-tCz and HATNA-tPCz.

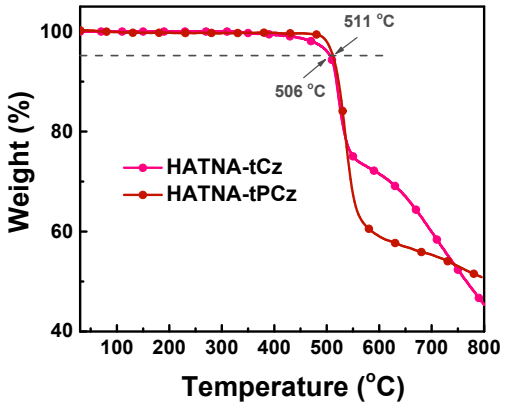

Fig. S8 TGA curves of HATNA-tCz and HATNA-tPCz.

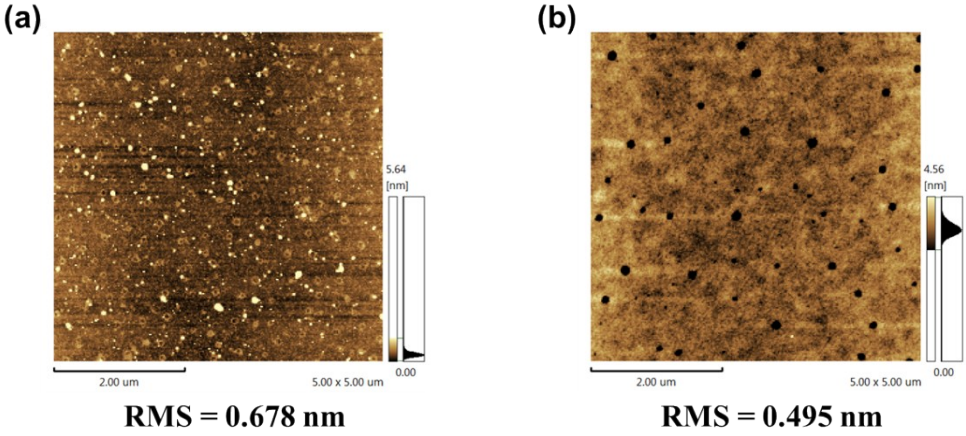

Fig. S9 AFM topographic images of the solution-processed (a) HATNA-tCz and (b) HATNA-tPCz neat films after drying at 50 °C.

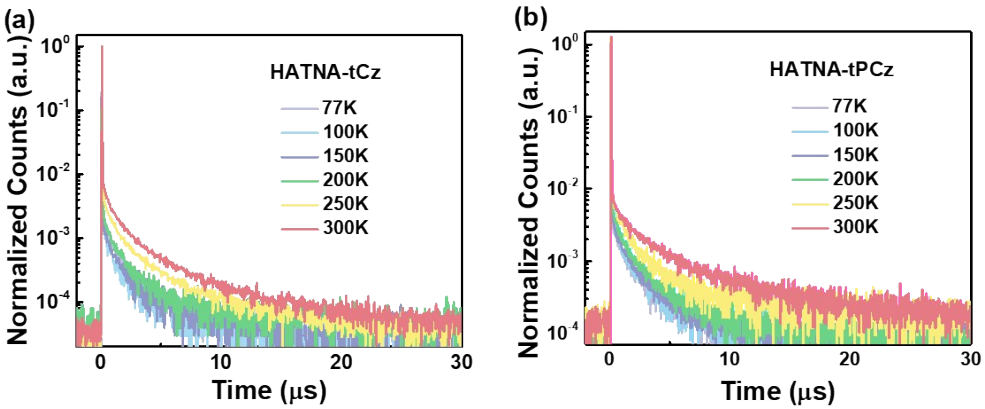

Fig. S10 The temperature-dependence transient photoluminescence decay curves of (a) HATNA-tCz and (b)HATNA-tPCz in the mCPCN host.

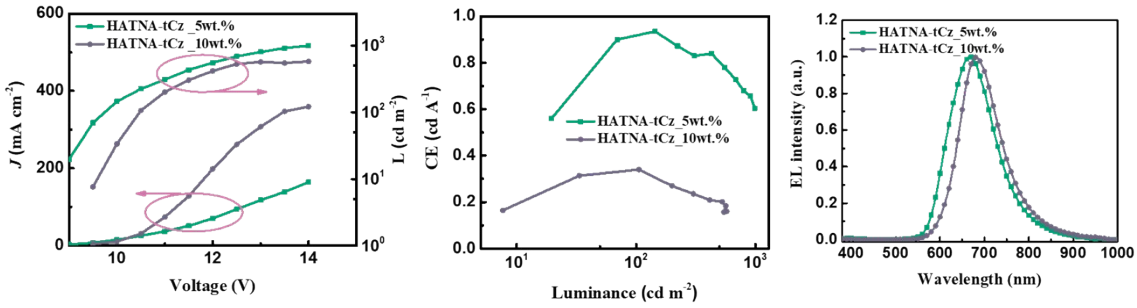

Fig. S11 The device performances based on HATNA-tCz with the doping concentrations of 5 wt.% and 10 wt.%

Table S1 The theoretical calculated data of HATNA-tCz and HATNA-tPCz

Compounds	HOMO [eV]	LUMO [eV]	E_g [eV][a]	S_1 [eV]	T_1 [eV]	ΔE_{ST} [eV]	f [b]
HATNA-tCz	-5.48	-3.05	2.43	2.22	1.89	0.33	0.33
HATNA-tPCz	-5.35	-3.24	2.11	1.94	1.86	0.08	0.23

[a] $E_g = -(E_{HOMO} - E_{LUMO})$. [b] Oscillator strength of the ground state to the lowest singlet excited states based on the DFT simulation.

Table S2 The fitting lifetimes and associated delayed fluorescence (DF) ratios of the two emitters

Compounds	Toluene [a]			Doped film [b]		
	τ_p [ns]	τ_d [μs]	DF ratio	τ_p [ns]	τ_d [μs]	DF ratio
HATNA-tCz	10.6	9.90	29%	14.0	5.81	66%
HATNA-tPCz	14.3	4.70	42%	15.7	4.94	62%

[a] Measured in toluene solutions (10^{-5} M) at room temperature. [b] Measured in 5 wt.% doped mCPCN films.

Table S3 Summary of the electroluminescence (EL) data of devices.

Devices	λ_{EL} [nm] [a]	CE_{max} [cd A^{-1}] [b]	PE_{max} [lm W^{-1}] [c]	EQE_{max} [%] [d]	CIE (x, y) [e]
HATNA-tCz_10 wt.%	682	0.34	0.10	1.2	(0.68, 0.32)
HATNA-tCz_5 wt.%	668	0.93	0.27	1.8	(0.65，0.34)
HATNA-tPCz_5 wt.%	692	1.54	0.54	4.8	(0.66，0.32)

[a] The EL emission peak at a driving voltage of 10 V. [b] Maximum current efficiency (CE_{max}). [c] Maximum power efficiency (PE_{max}). [d] Maximum external quantum efficiency (EQE_{max}). [e] The CIE at a driving voltage of 10 V.

Table S4 The summary of TADF-OLED characteristics from reported emitters with similar emissions in literatures. Device data are taken from Ref.

Compounds	Host	EQE_{max} [%]	CIE (x, y)/ λ_{EL} [nm]	Ref.
MPPA-Cz	Nondoped	0.064	(0.70, 0.29)/728	[1]
MPPA-3Cz	Nondoped	0.254	(0.69, 0.30)/715	
BF_2 dye	CBP (2 wt.%)	2.1	-/635	[2]
	CBP (60 wt.%)	0.4	-/716	
X (curcuminoid derivative)	CBP (6 wt.%)	9.69	721	[3]
2X (curcuminoid derivative)	CBP (2 wt.%)	5.1	758	[4]
HATNA-tPCz	**mCPCN (5 wt.%)**	**4.8**	**(0.66, 0.32)/692**	**This work**

References

[1] K. Sun, D. Chu, Y. Cui, W. Tian, Y. Sun and W. Jiang, *Org. Electron.*, 2017, **48**, 389-396.

[2] A. D'Aleo, M. H. Sazzad, D. H. Kim, E. Y. Choi, J. W. Wu, G. Canard, F. Fages, J. C. Ribierre and C. Adachi, *Chem. Commun.,* 2017, ***53***, 7003-7006.

[3] D. H. Kim, A. D'Aléo, X. K. Chen, A. D. S. Sandanayaka, D. Yao, L. Zhao, T. Komino, E. Zaborova, G. Canard, Y. Tsuchiya, E. Choi, J. W. Wu, F. Fages, J. L. Brédas, J. C. Ribierre and C. Adachi, *Nat. Photonics*, 2018, **12**, 98-104.

[4] H. Ye, D. H. Kim, X. Chen, A. S. Sandanayaka, J. U. Kim, E. Zaborova, G. Canard, Y. Tsuchiya, E. Y. Choi, J. W. Wu, F. Fages, J. L. Brédas, A. D'Aléo, J. C. Ribierre and C. Adachi, *Chem. Mater.*, 2018, **30**, 6702-6710.